Human Molecular Genetics, 2017, Vol. 26, No. 12 2321–2334

doi: 10.1093/hmg/ddx125
Advance Access Publication Date: 7 April 2017
Original Article

ORIGINAL ARTICLE

Mutant spastin proteins promote deficits in axonal transport through an isoform-specific mechanism involving casein kinase 2 activation

Lanfranco Leo[1,†], Carina Weissmann[2,†], Matthew Burns[2,†], Minsu Kang[2,3], Yuyu Song[3,4], Liang Qiang[1], Scott T. Brady[2,3], Peter W. Baas[1,*,‡] and Gerardo Morfini[2,3,*,‡]

[1]Department of Neurobiology and Anatomy, Drexel University College of Medicine, Philadelphia, PA, USA, [2]Department of Anatomy and Cell Biology, University of Illinois at Chicago, Chicago, IL, USA, [3]Marine Biological Laboratory, Woods Hole, MA, USA and [4]Department of Genetics, School of Medicine, Yale University, New Haven, CT, USA

* To whom correspondence should be addressed at: Department of Neurobiology and Anatomy, Drexel University College of Medicine, 2900 Queen Lane, Philadelphia, PA 19129, USA. Tel: 215 9918298; Fax: 215 8439082; Email: pbaas@drexelmed.edu (P.W.B.); Department of Anatomy and Cell Biology, 808 S. Woods St. Room 568, Chicago, IL 60612, USA. Tel: 312 9966869; Fax: (312)413-0354; Email: gmorfini@uic.edu (G.M.)

Abstract

Mutations of various genes cause hereditary spastic paraplegia (HSP), a neurological disease involving dying-back degeneration of upper motor neurons. From these, mutations in the *SPAST* gene encoding the microtubule-severing protein spastin account for most HSP cases. Cumulative genetic and experimental evidence suggests that alterations in various intracellular trafficking events, including fast axonal transport (FAT), may contribute to HSP pathogenesis. However, the mechanisms linking *SPAST* mutations to such deficits remain largely unknown. Experiments presented here using isolated squid axoplasm reveal inhibition of FAT as a common toxic effect elicited by spastin proteins with different HSP mutations, independent of microtubule-binding or severing activity. Mutant spastin proteins produce this toxic effect only when presented as the tissue-specific M1 isoform, not when presented as the ubiquitously-expressed shorter M87 isoform. Biochemical and pharmacological experiments further indicate that the toxic effects of mutant M1 spastins on FAT involve casein kinase 2 (CK2) activation. In mammalian cells, expression of mutant M1 spastins, but not their mutant M87 counterparts, promotes abnormalities in the distribution of intracellular organelles that are correctable by pharmacological CK2 inhibition. Collectively, these results demonstrate isoform-specific toxic effects of mutant M1 spastin on FAT, and identify CK2 as a critical mediator of these effects.

Introduction

Hereditary spastic paraplegias (HSP) represent a heterogeneous group of heritable diseases associated with progressive dying-back degeneration of upper motor neurons (1–3). From over fifty HSP-related genes identified to date, mutations in the *SPAST* gene encoding the protein spastin represent the most common form of HSP (*SPG4*-HSP) (4). Through an active mechanism

[†]The authors wish it to be known that, in their opinion, the first three authors should be regarded as joint First Authors.
[‡]The authors wish it to be known that, in their opinion, the last two authors should be regarded as joint Senior Authors.
Received: January 30, 2017. **Revised:** March 6, 2017. **Accepted:** March 24, 2017

involving ATP hydrolysis and oligomerization, spastin is known to sever microtubules into shorter pieces, facilitating their transport along axons for appropriate maintenance, remodeling and dismantling of the microtubule cytoskeleton (5–7). Critical for the severing activity of spastin are the microtubule-binding (MTBD) and AAA (ATPases Associated with Diverse Cellular Activities) domains (3). Based on homology analysis, a microtubule-interacting and endosomal trafficking (MIT) domain, two nuclear localization signals, and two nuclear export signals have also been reported, but their functional significance remains poorly understood (3,8). Translation of the *SPAST* gene at two different initiation codons results in the production of two major spastin isoforms, termed M1 and M85 in rodents or M1 and M87 in humans (8). Tissue expression analyses have found that, unlike the ubiquitous M87 isoform, the M1 spastin isoform is only detectable in the adult spinal cord, consistent with degeneration of corticospinal axons in *SPG4*-HSP (1,9). The unique 86 aminoacid stretch of M1 spastin includes several motifs that reportedly mediate interactions with various proteins, including the HSP-related GTPase atlastin, reticulons and REEP-1 (10,11). Through these interactions, M1 spastin has been proposed to coordinate microtubule-severing activity and membrane remodeling (2,12). However, isoform-specific functions of spastin remain unknown and the reasons for the restricted expression of the M1 isoform to adult spinal cord are similarly unclear.

The dying-back pattern of neuronal degeneration common to HSPs of different genetic etiology strongly suggests that HSP-related mutant proteins affect cellular processes critical for maintenance of the axonal compartment in affected neurons (1,2,13). Accordingly, several HSP genes encode proteins involved in intracellular trafficking events, including fast axonal transport (FAT) (2,14). Among these, the discovery of autosomal recessive mutations in the *SPG10* gene, which encodes the conventional kinesin heavy chain subunit *KIF5A*, provided direct evidence that even minor deficits in FAT suffice to produce HSP (15). Extending these findings to *SPG4*-HSP, several independent reports documented FAT deficits associated with *SPAST* mutations (9,16–19). However, mechanisms and specific molecular components linking mutant spastin proteins to these deficits remain elusive.

A large fraction of *SPAST* mutations are predicted to impair spastin severing activity and/or expression levels (20–22). Based on these observations, most reports to date have favored a haploinsufficiency mechanism underlying *SPG4*-HSP pathogenesis (23,24). However, several *SPG4*-HSP features, including its autosomal dominant pattern of inheritance, appear inconsistent with such a mechanism [reviewed in (3)]. Moreover, it is unclear how the loss of microtubule-severing activity would promote deficits in FAT (9).

Results from our prior work suggested a gain-of-function mechanism in *SPG4*-HSP. Specifically, we showed that truncated forms of M1, but not M85, mouse spastin polypeptides inhibit FAT in the isolated squid axoplasm (9). Given the restricted tissue distribution of M1 spastin to the adult spinal cord, such a mechanism appears consistent with both the increased vulnerability of upper motor neurons and the late onset characteristics of HSP (3,9). However, whether the findings of isoform-specific M1 spastin toxicity extended to *bona fide* HSP-related human mutant spastins was not addressed by these studies, and the mechanisms by which mutant M1 spastins inhibited FAT remained unknown.

Several misfolded neuropathogenic proteins have been shown to trigger alterations in FAT by promoting the abnormal activation of protein kinases involved in the phospho-regulation of motor proteins (25,26). Based on these precedents, we directly compared isoform-specific toxic effects of mutant spastins on FAT and further evaluated whether protein kinases could mediate such effects.

Results

M1, but not M87, human mutant spastin polypeptides inhibit fast axonal transport

Several issues complicate a *direct* comparison of mutant spastin isoforms effects on fast axonal transport (FAT) using mammalian cells. These include mutation-specific variations in spastin protein expression (22,27), and cell type-dependent variability of spastin isoform expression (9,22). In addition, transcriptional abnormalities associated with mutant spastin expression left unclear whether FAT deficits represent an epiphenomenon in *SPG4*-HSP (28,29). These issues are avoided using vesicle motility assays in the isolated squid axoplasm (30). First, the isolated squid axoplasm is a plasma membrane-free preparation, allowing direct perfusion of proteins and pharmacological inhibitors. Second, relative levels of perfused proteins can be tightly controlled, allowing for quantitative effect comparisons (31). Finally, neuronal cell bodies are absent from isolated axoplasm and thus, potential mechanisms involving nucleus-dependent activities (i.e., transcriptional alterations) can be ruled out. These unique features allowed us to directly evaluate and compare isoform-specific effects of HSP-related mutant spastin proteins on FAT.

Video-enhanced differential interference contrast microscopy allows precise measurement of FAT rates for MBOs moving in both anterograde and retrograde directions, which in the isolated axoplasm preparation are mainly carried by the multi-subunit motor proteins conventional kinesin and cytoplasmic dynein (CDyn), respectively (32,33). Perfusion of wild-type, catalytically active M1 and M85 full-length mouse spastins in axoplasm did not affect FAT (9). In contrast, truncated forms of M1, but not M85, mouse spastin inhibited both anterograde and retrograde FAT rates, suggesting isoform-specific toxic effects (3,9). Based on these precedents, we investigated whether these findings extended to human spastin proteins bearing *bona fide* HSP-related mutations. To this end, we generated cDNAs encoding M1 and M87 versions of human mutant spastins with a wide variety of *SPG4*-HSP mutations (Fig. 1A). STOP spastins, predicted to result from translation of some nonsense *SPAST* mutations (i.e., E114X), lack both MTBD and AAA domains (27,34). Because translation of spastin mRNAs containing nonsense mutations *in vivo* remains unclear (22), we also generated human spastin full-length constructs bearing HSP-causing missense mutations. The E442Q mutation, located within the AAA domain, was confirmed to abolish microtubule-severing activity (35), much as predicted for the closely located C448Y mutation (5,14). Mutations L195V and E112K, on the other hand, map to locations immediately adjacent to the MIT domain (22). *In vitro* translation (IVT) procedures were used to produce recombinant mutant spastin proteins, as before (9,36). Parallel IVT reactions in the presence of ^{35}S-radiolabeled methionine confirmed translation of recombinant spastin mutant proteins at the expected molecular weights (Fig. 1B).

Plots in Figures 2A–F and Supplementary Material, Figure S1 show results from vesicle motility assays following perfusion of human M87 and M1 mutant spastin polypeptides. Perfusion of axoplasms with human M87-STOP spastin did not affect FAT

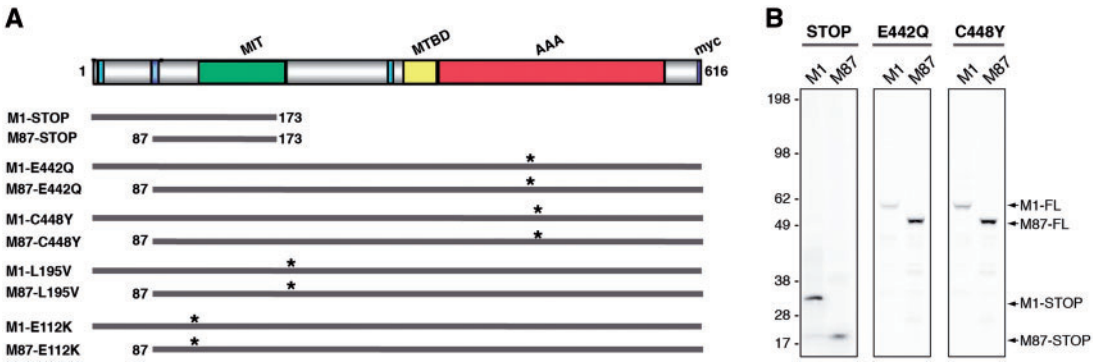

Figure 1. Recombinant mutant spastin proteins in this study. (**A**) Schematic representation of mutant spastin proteins used in this study. Specific domains are indicated in the top graph including ATPase associated with various cellular activities (AAA, in red), microtubule-interacting and trafficking (MIT, in green) and microtubule-binding (MTB, in yellow) domains. Nuclear localization signals (NL, dark blue), a nuclear export (NLS, light blue) and a carboxy-terminal *myc* tag (in purple) are shown. Asterisks indicate the approximate location of missense mutations. Note that truncated M1-STOP and M87-STOP lack both AAA and MTBD domains. (**B**) *In vitro* translation of STOP, E442Q, and C448Y cDNA spastin constructs was performed in the presence of ^{35}S-methionine. Reactions were separated by SDS-PAGE and analyzed using Phospho-imager scanning. Representative autoradiograms confirm expression of M1 and M87 mutant spastin proteins at the predicted molecular weights. Control reactions lacking plasmid cDNA did not result in detectable protein synthesis (not shown).

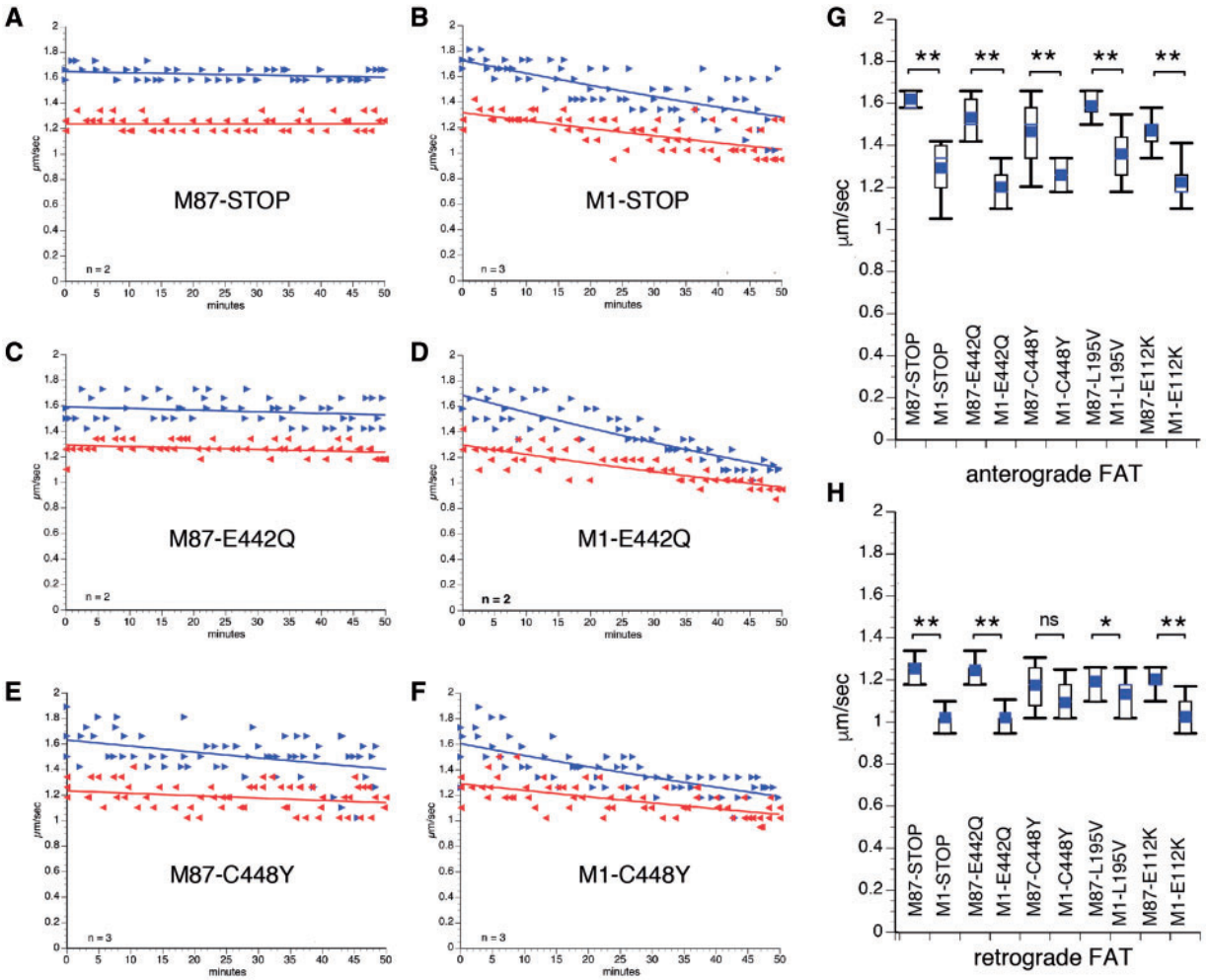

Figure 2. Mutant M1, but not M87 spastins inhibit FAT. Plots in A–F depict results from vesicle motility assays in isolated squid axoplasm. *In vitro* translated mutant spastins were perfused into axoplasm and fast axonal transport (FAT) rates monitored by video microscopy. Individual rate measurements (µm/s, arrowheads) are plotted as a function of time (minutes). Both anterograde (blue arrowheads and lines) and retrograde (reverse red arrowheads and lines) FAT rates are shown in each plot. Perfusion of human M87-STOP (**A**), M87-E442Q (**C**), and M87-CY448 (**E**) mutant spastins showed no effect on FAT. In contrast, a marked inhibition of both anterograde (conventional kinesin-dependent) and retrograde (cytoplasmic dynein-dependent) FAT rates was observed after perfusion of their corresponding isoform counterparts M1-STOP (**B**), M1-E442Q (**D**) and M1-C448Y (**F**). Plots showing quantitation of average anterograde (**G**) and retrograde (**H**) FAT rates obtained 30-50 minutes after spastin perfusion indicates that inhibition of FAT represents an isoform-specific toxic effect of all mutant M1 spastins tested. *n*: number of independent experiments; *ns*: not significant; $^{*}P < 0.05$; $^{**}P < 0.0001$.

(Fig. 2A). In contrast, a marked inhibition of both anterograde and retrograde FAT rates was observed for axoplasms perfused with M1-STOP spastin (Fig. 2B), consistent with prior results using mouse M1-STOP spastin (9). These toxic effects were also elicited by full-length M1 spastin proteins bearing the mutations E442Q (Figs 2D), C448Y (Fig. 2F), L195V (Supplementary Material, Fig. S1B) and E112K (Supplementary Material, Fig. S1D), but not by M87 spastin proteins bearing the same mutations (Fig. 2C and E, and Supplementary Material, Fig. S1A and S1C). Quantitation of average FAT rates obtained 30–50 min after perfusion of spastin proteins confirmed a dramatic reduction in anterograde FAT rates for axoplasms perfused with M1 mutant spastins, compared to their M87 isoform counterparts (Fig. 2G and Supplementary Material, Table S1). Retrograde FAT rates were also reduced in mutant M1 spastin-perfused axoplasms, although the extent of this inhibitory effect was somewhat more variable among the mutant M1 spastin proteins tested (Fig. 2H and Supplementary Material, Table S1). Collectively, these results indicate that inhibition of FAT represents a toxic effect triggered by mutant M1, but not mutant M87 spastin proteins. Moreover, these effects were independent of transcriptional alterations as well as microtubule-binding and severing activities.

M1-STOP, but not M87-STOP expression, promotes cellular phenotypes associated with abnormalities in intracellular trafficking

We then evaluated the relevance of findings in Figure 1 to mammalian cells. To circumvent technical issues associated with limited transfection efficiency and to allow parallel live-cell imaging and biochemical studies of homogeneous cell populations, we established SH-SY5Y neuroblastoma cell monoclones stably expressing M87-STOP or M1-STOP spastins, as described in Supplementary Materials.

Naïve, M87-STOP, and M1-STOP SH-SY5Y cells were transfected with plasmids encoding RFP-tagged synaptophysin (RFP-syn) and live-cell imaging experiments were performed to determine the relative proportions of motile RFP-syn-positive vesicles among these experimental groups (Fig. 3A and B). Consistent with findings from isolated squid axoplasm, a marked reduction in the percentage of motile RFP-syn-positive vesicles was observed in M1-STOP cells (42.5 ± 5.5% of the total) compared to both M87-STOP and GFP-transfected (control) cells (69.4 ± 5.6% and 78.3 ± 6.2% respectively), suggesting intracellular transport impairments in cells expressing M1-STOP. In addition, immunocytochemical methods were used to evaluate alterations in Golgi apparatus distribution, as this organelle undergoes aberrant dispersion following alterations in conventional kinesin or CDyn function (37,38) (Fig. 3C and D). In both naïve and M87-cells, the Golgi apparatus displayed a typical clustered, perinuclear distribution, comprising 3.9 ± 0.38% and 3.8 ± 0.49% of the total cellular area, respectively. In contrast, a marked dispersion of this organelle was observed in M1-STOP cells (5.6 ± 0.38% of total cellular area), suggesting functional impairment of motor proteins.

Increased phosphorylation of motor proteins in association with mutant M1 expression

Several unrelated neuropathogenic polypeptides have been shown to produce FAT deficits by triggering abnormal activation of kinases involved in phospho-regulation of motor proteins (25,26). Consistent with these findings, mutant M1 spastins

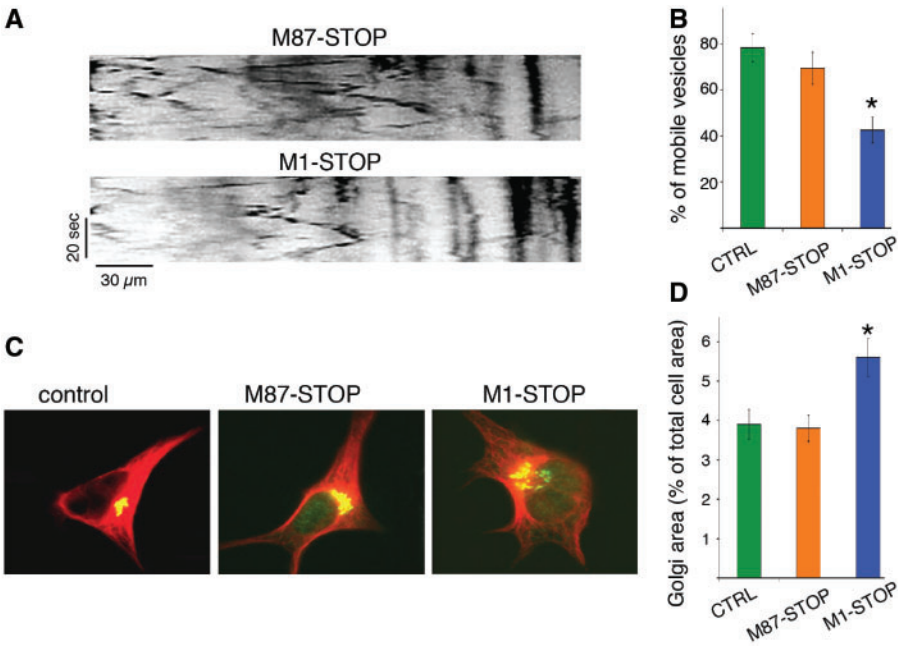

Figure 3. Abnormal transport and distribution of organelles in SH-SY5Y cells expressing M1-STOP spastin. SH-SY5Y cells stably expressing M1-STOP and M87-STOP spastins (see Supplementary Materials) were transfected with plasmids encoding an RFP-tagged version of synaptophysin (RFP-syn). The proportion of RFP-syn-positive mobile vesicles in neurites was analyzed using live-cell imaging, and representative kymographs are shown in **(A)** for comparison. **(B)** Compared to control (ctrl, GFP-transfected) cells, M87-STOP cells showed similar fraction of mobile RFP-syn-positive vesicles (78.3±6.2% *vs* 69.4 ± 5.6%). In contrast, M1-STOP cells showed a marked reduction in the proportion of these vesicles (42.5±5.5%). **(C)** Representative images of SH-SY5Y cells showing immunoreactivity for the cis Golgi marker GM130 (in green) and tubulin (in red). **(D)** Quantitation of GM1-130 immuno-positive area/total cell area revealed a wider distribution of the Golgi apparatus in M1-STOP cells (5.6±0.38%), compared to both control (3.9±0.38%) and M87-STOP cells (3.8±0.49% respectively). *$P < 0.05$. Bar, 10 microns.

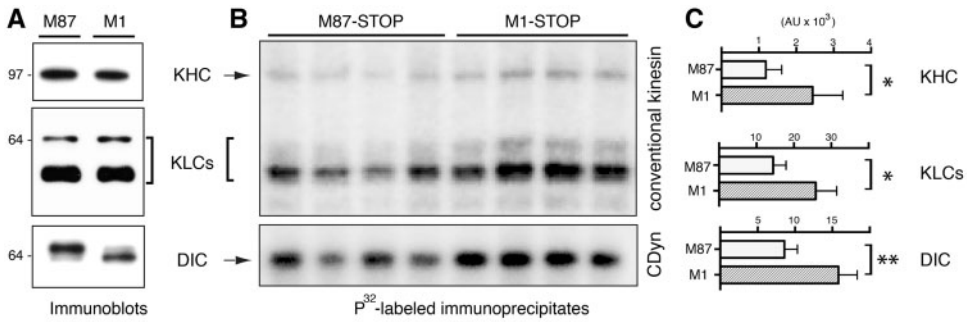

Figure 4. Increased phosphorylation of motor proteins in association with M1-STOP expression. Stably-transfected SH-SY5Y cells expressing M1-STOP and M87-STOP were metabolically labeled using radiolabeled ^{32}P. Lysates derived from these cells were processed for immunoprecipitation using antibodies that selectively immunoprecipitate the multi-subunit motor proteins conventional kinesin and cytoplasmic dynein (CDyn). (**A**)) Immunoblot analysis confirmed similar expression levels of KHCs and KLCs subunits of conventional kinesin, as well as DIC subunits of cytoplasmic dynein (CDyn) between M1-STOP (M1) and M87-STOP (M87) cells. (**B**) Autoradiogram analysis of ^{32}P-labeled conventional kinesin and CDyn immunoprecipitates revealed increased phosphorylation of kinesin heavy (KHC) and light chain (KLCs) subunits, as well as dynein intermediate chain (DIC) subunits in cells expressing M1-STOP, compared to M87-STOP cells. (**C**) Phospho-imager-based quantitation of data in B. $^{*}P < 0.05$; $^{**}P < 0.01$.

inhibited FAT in the axoplasm preparation at concentrations several orders of magnitude lower than endogenous tubulin [approx. 50 μM, (31)], suggesting an enzymatic mechanism rather than steric effects. This observation, and results from experiments in Figure 3 prompted us to evaluate potential alterations in the phosphorylation of the major FAT multi-subunit motor proteins conventional kinesin and CDyn in M1-STOP cells (Fig. 4). To this end, M1-STOP and M87-STOP cells were metabolically labeled with ^{32}P and lysed after 4 h. Clarified lysates were subject to immunoprecipitation using antibodies that effectively immunoprecipitate conventional kinesin (39) and CDyn (40) holoenzymes. Immunoblot analysis revealed similar expression levels of heavy (KHC) and light chain (KLC) subunits of conventional kinesin among M1-STOP and M87-STOP cells. Similarly, M87-STOP and M1-STOP cells expressed similar levels of the major CDyn phosphoprotein subunit dynein intermediate chain (DIC) (Fig. 4A). In contrast, autoradiogram and phospho-imager-based analysis revealed increased phosphorylation of these motor protein subunits in M1-STOP cells, compared with M87-STOP cells (arbitrary units: KHC: 2435 ± 806 vs 1185 ± 424; KLC: 25860 ± 5604 vs 14468 ± 3441; DIC: 15832 ± 2500 vs 8588 ± 1731; respectively) (Figs 4B and C). Autogradiogram analysis of whole cell lysate aliquots prior to immunoprecipitation confirmed similar inputs of ^{32}P-radiolabeled protein (not shown). Together, these observations revealed increased phosphorylation of FAT motor proteins in M1-STOP-expressing cells.

Casein Kinase 2 mediates the toxic effect of mutant M1 spastins on FAT

Based on results from experiments in Figure 4, co-perfusion experiments in isolated squid axoplasm were used to determine whether specific protein kinases mediated the toxic effect of mutant M1 spastins on FAT. From several protein kinases tested in this preparation, casein kinase 2 (CK2) was previously found to inhibit both anterograde and retrograde FAT (41,42), a pattern of inhibition similar to that elicited by mutant M1 spastins. Further, CK2 was previously shown to phosphorylate KHC, KLC, and DIC subunits (41,43–45), prompting us to evaluate whether this kinase mediated the toxic effect of mutant M1 spastins on FAT (Fig. 5). M1-STOP protein was co-perfused with tetrabromocinnamic acid (TBCA, 200 nM), a highly specific pharmacological CK2 inhibitor (46). TBCA blocked the toxic effect of M1-STOP on FAT in co-perfusion experiments (Fig. 5A, compare to Fig. 2B). Ruling out off-target effects of TBCA, a CK2 peptide substrate (CK2pept; 500 μM), which acts as a competitive CK2 inhibitor in the axoplasm preparation (41), also prevented the inhibitory effect of M1-STOP on FAT (Fig. 5B), as did the structurally unrelated CK2 inhibitor DMAT [5 μ (47)] (data not shown). In addition, TBCA co-perfusion also prevented the inhibitory effects of M1-E442Q (Fig. 5C, compare to Fig. 2D) and M1-C448Y (Fig. 5D, compare to Fig. 2F) on FAT. Quantitation of average FAT rates 30–50 min after perfusion confirmed that CK2 activation mediates the toxic effect of several different mutant M1 spastins on FAT (Fig. 5E and F and Supplementary Material, Table S1). Together, these results suggest that the toxic effect of mutant M1 spastins on anterograde and retrograde FAT involves CK2 activation.

In vivo, CK2 exists as a tetrameric protein comprised of two catalytic subunits (α and/or α'), and two regulatory β subunits [reviewed in (48)]. Based on results from Figure 5, we performed CK2 activity assays using lysates prepared from M87-STOP and M1-STOP cells. Despite similar levels of CK2 α, α' and β subunit mRNA and protein expression (Supplementary Material, Fig. S3), lysates prepared from M1-STOP cells displayed increased levels of CK2 activity, compared to lysates prepared from M87-STOP cells (Fig. 6A). Based on these results, we then explored the contribution of CK2 to aberrant cellular phenotypes elicited by M1-STOP spastin expression in mammalian cells.

To evaluate whether CK2 mediated the impairments in RFP-syn mobility documented in Figure 3A and B, naïve, M87-STOP and M1-STOP cells were treated with TBCA. As shown in Figure 6B and C, the fraction of RFP-syn-positive mobile MBOs was significantly increased in M1-STOP cells treated with TBCA, compared to M1-STOP cells treated with DMSO vehicle (59.4 ± 5.9%*vs* 42.5 ± 5.5%, respectively). TBCA treatment did not affect the fraction of RFP-syn-positive mobile vesicles in either M87-STOP or naïve cells (M87-STOP + DMSO: 69.4 ± 5.6%; M87-STOP + TBCA: 66.2 ± 6.3%; naïve + DMSO: 78.3 ± 6.2%; naïve + TBCA: 65.4 ± 6.9%). In addition, TBCA treatment also restored the aberrant dispersion of the Golgi apparatus observed in M1-STOP cells to control levels (% of the total cell area; M1-STOP + TBCA: 3.8 ± 2.6% *vs* M1-STOP + DMSO: 5.6 ± 0.38%). Treatment of M87-STOP and naïve cells with TBCA showed no significant effect on the Golgi distribution (3.8 ± 0.27% vs 3.6 ± 0.33% of the total cell area, respectively). Together, these experiments suggest that CK2 mediates the

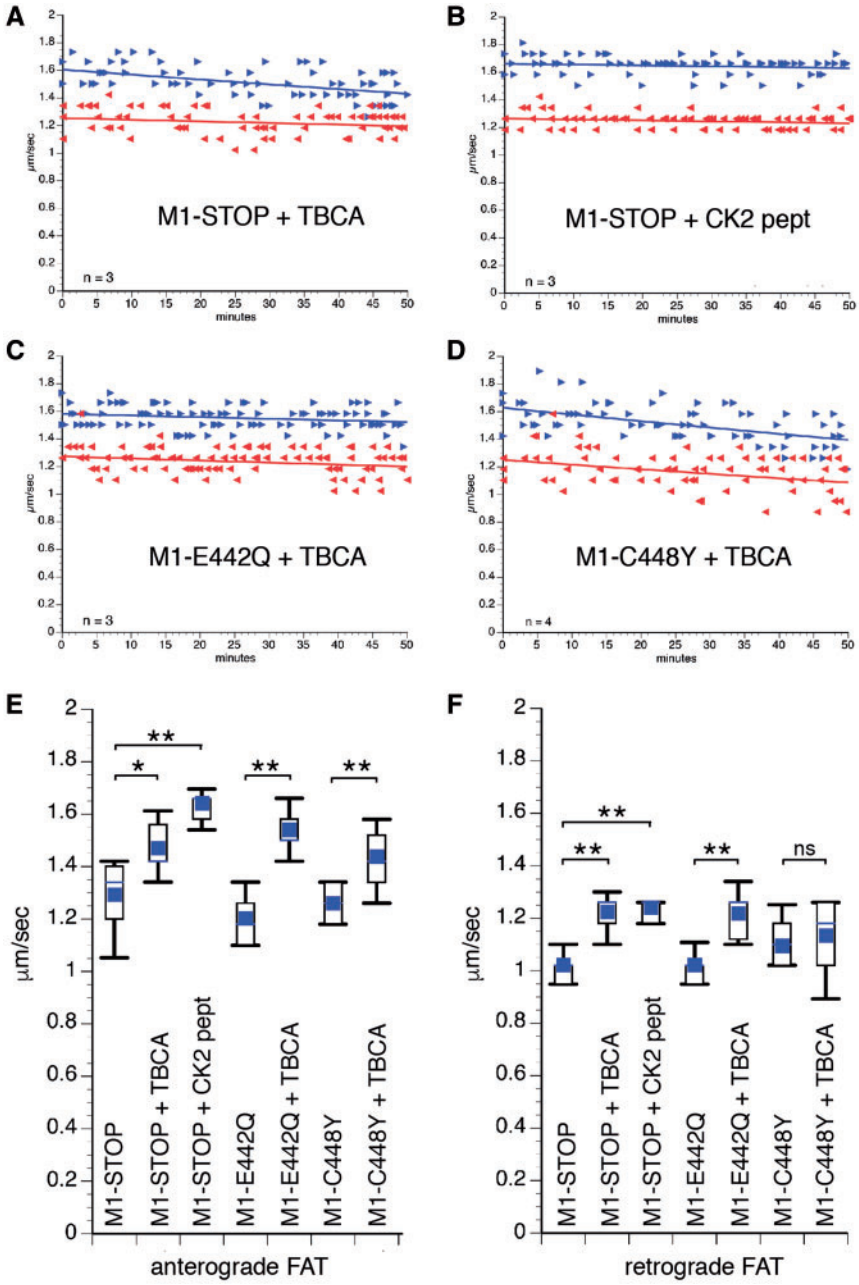

Figure 5. Casein Kinase 2 mediates the toxic effect of mutantM1 spastins on fast axonal transport (FAT). Plots in A–D depict results from co-perfusion experiments using vesicle motility assays in isolated axoplasm, as in Figure 2. (**A**) When co-perfused with recombinant M1-STOP, the highly selective CK2 inhibitor TBCA (200nM) completely prevented the toxic effect of M1-STOP on FAT (compare to Fig. 2B). (**B**) Ruling out off-target effects of TBCA, a CK2-specific peptide substrate (CK2pept, 500 µM), which acts as a competitive inhibitor in these assays, also blocked this toxic effect. TBCA also prevented the inhibitory effect of M1-E442Q (C; compared to Fig. 2D) and M1-C448Y (**D**; compare to Fig. 2F) on FAT. Statistical analysis of anterograde (**E**) and retrograde (**F**) FAT rates indicate that CK2 activation represents an effect common to mutant M1 spastin proteins bearing different mutations. n: number of independent experiments. ns: not significant; $^{*}P < 0.001$; $^{**}P < 0.0001$.

toxic effect of M1-STOP on RFP-syn motility and Golgi distribution.

Tubulin modification status accompanying mutant spastins

We also evaluated whether alterations in tubulin post-translational modifications could contribute to the intracellular trafficking deficits observed in M1-STOP cells by using quantitative immunocytochemistry and immunoblotting methods, as before (49) (Supplementary Material, Fig. S2). These studies were done because levels of post-translationally detyrosinated and/or acetylated tubulins reportedly modulate the interaction of microtubules with various proteins, including molecular motors [discussed in (3)]. Results from these experiments revealed similar levels of acetylated microtubules among naïve, M87-STOP, and M1-STOP cells (Supplementary Material, Fig. S2E and F). Analysis of microtubule tubulin tyrosination shows approximately 30% increase in M1 STOP cells (2.6 ± 0.11), while GFP- or M87-STOP expressing cells have a slightly lower value (GFP + DMSO: 1.94 ± 0.11 and M87-STOP + DMSO: 1.92 ± 0.15,

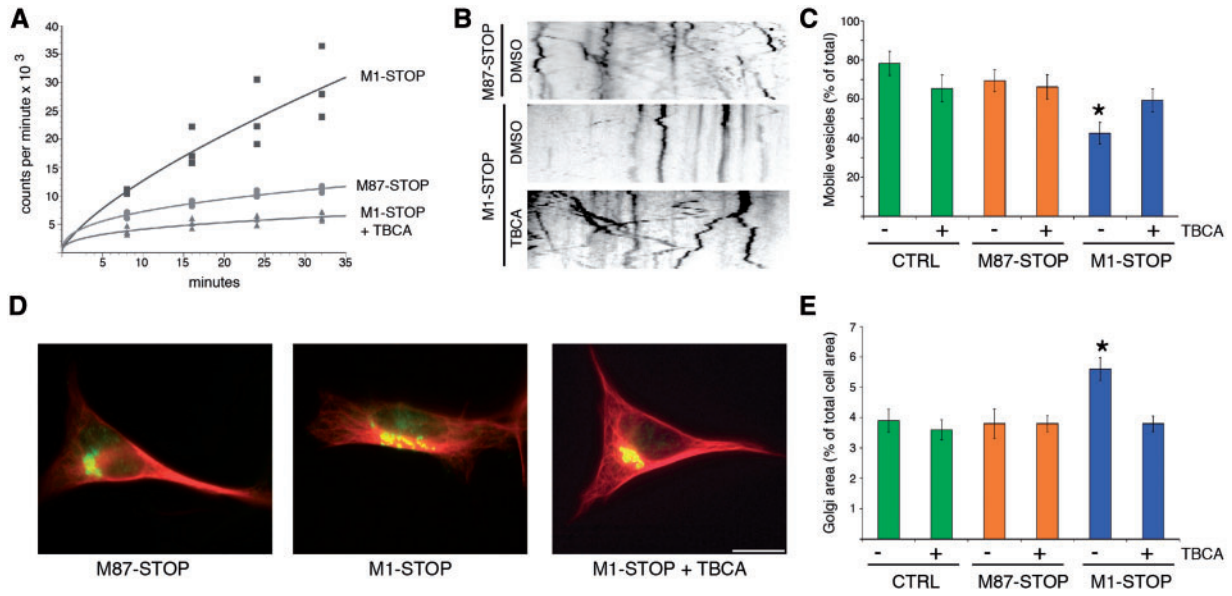

Figure 6. CK2 mediates aberrant mammalian cell phenotypes induced by M1-STOP expression. (**A**) Kinase assays using CK2 peptide substrate as a phosphate acceptor showed increased levels of active CK2 in lysates prepared from M1-STOP cells, compared to M87-STOP cells. Addition of the CK2 inhibitor TBCA to M1-STOP lysates confirmed specificity of the kinase reaction for CK2. (**B**) Representative kymographs showing transport of vesicles containing RFP-synaptophysin in control (CTRL, naïve cells), M87-STOP and M1-STOP SH-SY5Y cells. (**C**) Compared to DMSO vehicle-treated CTRL (78.3±6.2%) and M87-STOP cells (69.4 ± 5.6%), a marked reduction in the proportion of mobile vesicles was observed in DMSO-treated M1-STOP cells (42.5±5.5%). However, this reduction was completely blocked in M1-STOP cells treated with TBCA(59.4±6.0%). Notably, TBCA did not markedly affect the proportion of motile vesicles in CTRL (65.4±6.9%) or M87-STOP cells (66.2±6.3%). (**D**) Representative images of SH-SY5Y cells showing immunoreactivity for the cis Golgi marker GM130 (in green) and tubulin (in red). (**E**) Quantitation of GM1-130 immunopositive area/ total cell area shows similar values for GFP-transfected (naïve, 3.9±0.38%) and M87-STOP (3.8±0.49%) cells treated with DMSO (vehicle).These values were not significantly affected by TBCA treatment (naïve + TBCA: 3.6±0.33%, M87-STOP + TBCA: 3.8±0.27%). In contrast, a marked dispersion of the Golgi apparatus was observed in DMSO-treated M1-STOP cells (5.6±0.38%), which was completely blocked by TBCA treatment (3.8±0.26%). *$P < 0.05$. Bar, 10 microns.

respectively)] (Supplementary Material, Fig. S2A–D). Without affecting the tubulin tyrosination levels of any other experimental group, TBCA restored to normal the elevated levels observed in the M1-STOP cells. (M1-STOP + TBCA: 2.1 ± 0.10; M87-STOP + TBCA: 2.0 ± 0.10; GFP + TBCA: 1.95 ±0.08) or acetylation (graphs in Supplementary Material, Fig. S2D and F, respectively). Collectively, these results suggest that the toxic effects of M1-STOP on RFP-syn transport and Golgi apparatus distribution documented in Figure 3 did not result from alterations in tubulin acetylation, but may relate to changes in tubulin tyrosination.

Altered Mitochondrial redistribution associated with mutant M1 spastin expression is correctable by CK2 inhibition

Finally, we evaluated whether the findings of isoform-dependent spastin toxicity could be observed in other cell types, including primary rat cortical neurons. For these studies, we focused on mitochondria, whose intracellular distribution is reportedly compromised by mutant spastin (17,19) (Fig. 7). Initial studies used RFL-6 fibroblasts, a cell line well suited for imaging of mitochondria because of its flat morphology (Fig. 7A–E). In a typical fibroblast, most mitochondria are asymmetrically clustered in one pole of the cell, with a smaller fraction dispersed in the remaining regions. By labeling mitochondria with the fluorescent probe orange Mitotraker®, we observed that a high percentage of control (RFP-transfected) cells have mitochondria that follow this distribution pattern and a relatively small fraction have mitochondria not asymmetrically clustered in this fashion (RFP + DMSO: 31.2 ±2.1% cells with dispersed mitochondria). Ectopic expression of RFP and M87-C448Y (with IRES) had little or no effect on mitochondrial distribution (M87-C448Y + DMSO: 41.0±4.2% cells with dispersed mitochondria), with no statistical difference between these groups. In contrast, expression of RFP and M1-C448Y notably increased the number of cells that had dispersed mitochondria (M1-C448Y + DMSO: 62.0±3.6%). Treatment with TBCA did not detectably alter mitochondrial distribution in cells expressing RFP alone or in cells expressing RFP with M87-C448Y (RFP + TBCA: 30.6±11.7%, M87-C448Y + TBCA: 40.6 ±10.6% cell with dispersed mitochondria). TBCA lowered the number of cells with dispersed mitochondria (M1-C448Y + TBCA: 38.6±6.7%) to levels similar to the M87-C448Y or RFP cells. As with the fibroblasts, M1-C448Y caused mitochondrial redistribution in primary cortical rat neurons (Fig. 7F–J) (M1-C448Y + DMSO: 63.3±3.2% cells with dispersed mitochondria), compared to RFP cells or M87-C448Y cells (RFP + DMSO: 25.3±4.4% and M87-C448Y + DMSO: 37.0±4.0% cells with dispersed mitochondria of the total). Treatment with TBCA reduced the number of M1-C448Y cells with dispersed mitochondria (M1-C448Y + TBCA: 38.0±2.7%) but did not significantly affect the other groups (M87-C448Y + TBCA: 32.7±3.5%; RFP + TBCA: 14.0±11.3%).

Discussion

Over 200 *SPAST* mutations including missense, nonsense, and single amino acid substitutions have been associated with *SPG4*-HSP (4,27). Because most pathogenic *SPAST* mutations are predicted to compromise severing activity and/or expression

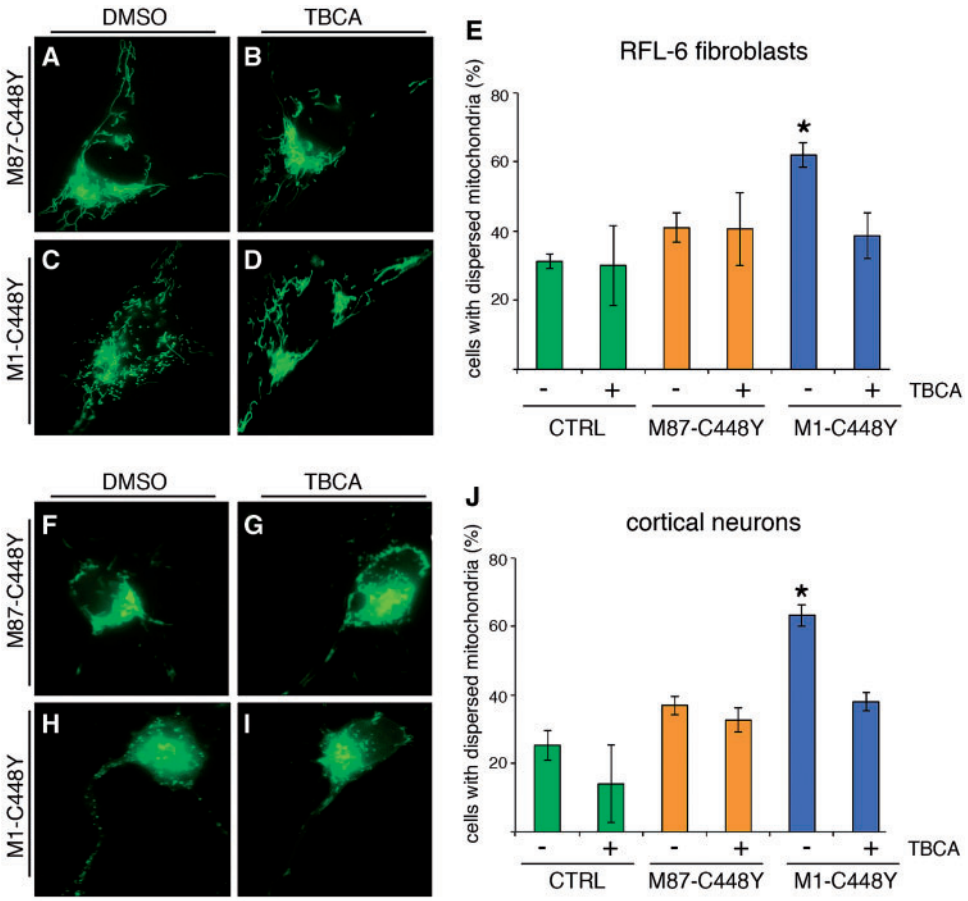

Figure 7. M1-C448Y spastin alters mitochondrial distribution in a CK2-dependent manner. **(A–D)** Analysis of mitochondrial distribution in RFL-6 rat fibroblasts under various experimental conditions, while **(F–I)** are the same experimental conditions but with primary rat cortical neurons. (A,F) are cells expressing M87-C448Y under treatment with DMSO, the vehicle-control. (B,G) are cells expressing M87-C448Y under treatment with TBCA. (C,H) are cells expressing M1-C448Y under treatment with DMSO, the vehicle-control. (D,I) are cells expressing M87-C448Y under treatment with TBCA. In both cell types, M1-C448Y caused mitochondrial dispersion, but M87-C448Y did not. TBCA had no effect on mitochondrial distribution in cells expressing M87-C448Y, but reverted the mitochondrial dispersion back to the control pattern in cells expressing M81-C448Y. Quantitative data are shown for RFL-6 fibroblasts **(E)** and neurons **(J)**. See *Results* for numerical data. *$P < 0.05$. Bar, 10 microns.

levels, haploinsufficiency remains the prevalent mechanistic explanation for the disease (22). For example, nonsense *SPAST* mutations have been proposed to compromise mRNA stability, which would theoretically result in little or no truncated spastin protein expression (22,50). Moreover, the entire *SPAST* gene may be deleted in some HSP patients (51), although this possibility is based on exon mapping data rather than genome sequencing. These and other reports fueled the notion that *SPG4*-HSP neuropathology results from reductions in spastin-dependent microtubule severing (20,21). However, multiple observations call into question haploinsufficiency as a sufficient mechanistic explanation for the disease. For example, no correlation has been found between the degree to which mutations compromise spastin microtubule-severing activity and disease onset or severity (24,27,52). Also, reports on the lack of detectable truncated spastin proteins from *SPG4*-HSP patient samples have been limited to non-neuronal cells, which only express M87 spastin (53). Of note, the only *SPG4*-HSP post-mortem spinal cord tissue sample analyzed by immunoblot to date showed a major band corresponding to mutant M1 (54), suggesting that mutant M1 proteins may accumulate over time. Supporting this possibility, we found that, despite equivalent levels of mutant M1-STOP and M87-STOP mRNA expression in our stable SH-SY5Y spastin cell lines, the mutant M1-STOP protein showed increased stability or accumulation (Supplementary Material, Fig. S2B). Also, some neuropathogenic proteins, including mutant superoxide dismutase 1 (55) and a polyglutamine-expanded mutant huntingtin fragment (56), have been shown to promote neuronal degeneration at expression levels too low to be detected by conventional immunoblotting techniques. These precedents raise the possibility that the pathology associated with nonsense *SPAST* mutations could be triggered by very low amounts of translated mutant M1 spastin protein. As for the situation with *SPAST* deletions, such deletions often lead to expression of aberrant fusion proteins involving neighboring genes, which could contribute to the neuropathology (57).

Various cellular and animal models have been generated to address *SPG4*-HSP pathogenesis including two mouse, a zebrafish, a worm, and various *Drosophila* models (19,58,59,60–62). These models were all based on complete or partial spastin knockdown, rather than on *SPAST* mutations. Although clearly well suited for an evaluation of spastin's basic function(s), claims of relevance to *SPG4*-HSP pathogenesis are circular in their logic, as they assume haploinsufficiency as the underlying mechanism. Highlighting this issue, expression of ectopic human mutant spastins in *Drosophila* caused a much stronger HSP-like phenotype than endogenous spastin knockout did (63), and similar observations were found in cultured mammalian

neurons (9,63–65). Recently, a mild HSP-like gait phenotype was described for homozygous mice where the HSP-related mutation N384K was introduced in the endogenous mouse *SPAST* gene (66). If this phenotype resulted from reductions in spastin severing activity, complete deletion of spastin would be expected to promote an even stronger phenotype. However, no obvious HSP-related phenotypes were found for the two *SPAST* knockout mouse models reported to date (59,19).

Several HSP-related mutant gene products have been directly or indirectly linked to various intracellular trafficking events, including FAT [reviewed in (2)], and the dying-back pattern of neuronal degeneration observed in HSP is consistent with the critical dependence of axons on these events (1,26). Interestingly, several independent reports documented deficits in FAT in association with mutant spastin expression (16–19). As discussed above, reductions in microtubule severing have often been assumed to underlie such deficits, but results from the present work suggest an alternative isoform-specific toxic gain-of-function mechanism. Specifically, squid axoplasm experiments demonstrate that human M1, but not M87, spastin polypeptides bearing a wide variety of unrelated mutations (STOP, E442Q, C448Y, E112Q, and L195I) all similarly inhibit FAT. This common toxic effect of M1 mutant spastins was independent of severing activity, as it was elicited by mutant STOP proteins and by catalytically inactive M1-E441Q and CY448 spastins. That only mutant M1, but not M87, spastins inhibited FAT strongly suggests a critical role of M1's unique 86-amino acid stretch on this effect. Given the restricted distribution of M1 spastin to adult spinal cord (9), findings of isoform-dependent mutant spastin toxicity bear relevance for the selective cellular topography and late onset characteristics of HSP (26).

Observations of selective mutant M1 spastin toxicity in isolated axoplasm are also consistent with abnormal cellular phenotypes elicited by M1-STOP, but not M87-STOP in mammalian cells. Specifically, a marked reduction in the proportion of RFP-syn-positive mobile vesicles was observed in association with M1-STOP expression. In addition, M1-STOP, but not M87-STOP cells showed aberrant localization of the Golgi apparatus, whose degree of dispersion involves the coordinated activities of conventional kinesin and CDyn (37,38). Extending these results, cultured neurons expressing the HSP-related mutant M1-C448Y, but not M87-CY448Y, displayed abnormal distribution of mitochondria, as reported for other spastin mutations (67).

It was previously proposed that mutant spastins compromise interactions between molecular motors and microtubules by coating the surface of the microtubule (67). However, mutant M1-STOP spastin lacking MTB and AAA domains also inhibited FAT in isolated axoplasm. Furthermore, this inhibitory effect was elicited at concentrations orders of magnitude lower than endogenous squid microtubules, suggesting an enzymatic mechanism rather than steric interference. As observed with mutant M1 spastin, several neuropathogenic misfolded proteins including tau (68), huntingtin (36), and superoxide dismutase 1 (69), were previously shown to inhibit FAT in squid axoplasm by activating specific protein kinases involved in the phosphoregulation of motor proteins. Highlighting the relevance of these experiments to disease-related neuronal dysfunction, these proteins promoted disease-relevant pathogenic events (i.e.; axonal pathology) in living cells that were correctable by specific protein kinase inhibitors. Accordingly, metabolic labeling experiments in the present study revealed increased phosphorylation of conventional kinesin and CDyn subunits in M1-STOP cells, compared to M87-STOP cells. Co-perfusion experiments in isolated axoplasm further revealed CK2 as a critical kinase mediating the inhibitory effects of mutant M1 spastin on FAT, as several structurally unrelated CK2 inhibitors consistently blocked this toxic effect. Kinase assays revealed increased levels of active CK2 activation in M1-STOP, compared to M87-STOP cells, while TBCA treatment prevented abnormal phenotypes of M1-STOP cells and corrected the aberrant distribution of mitochondria observed in M1-C448Y-expressing cultured neurons.

How do mutant spastin polypeptides activate CK2? Although CK2 has been historically described as a constitutively active protein kinase, several regulatory mechanisms for this kinase have been identified, including targeting to specific substrates by interacting proteins, phosphorylation by other protein kinases, and alterations in inhibitory α/β subunit interactions (70–74). Polybasic ligands including polylysine, putrescine and spermine and some endogenous cellular proteins are known to affect intramolecular inhibitory α/β subunit interactions and activate CK2 through this later mechanism (70). Interestingly, the 86 amino acid amino terminal domain unique to M1 spastin contains a highly positive net charge (pI = 11.83), as well as a highly basic amino acid stretch rich in lysines. These observations are consistent with the hypothesis that the unique amino terminal domain of M1 spastin may directly activate CK2, but additional experiments are needed to evaluate this possibility.

Relevant to the mode of M1 spastin-induced CK2 activation, it is noteworthy that wild-type, catalytically active M1 spastin does not affect FAT in isolated axoplasm (9). This observation, and data in this manuscript are consistent with the hypothesis that different *SPAST* mutations similarly promote increased exposure of M1 spastin's unique 86 amino acid sequence, making it available for direct or indirect interactions with CK2. Such aberrant exposure could result from mechanisms involving: 1) a common conformational change induced by unrelated mutations; or 2) reduced interaction with specific binding partners. Precedents for the former mechanism have been reported for disease-related forms of tau, whose toxic effects on FAT were shown to depend on exposure of a short amino terminal sequence termed the PAD domain (68). Supporting the second possibility, *SPAST* mutations reportedly compromise an interaction between the unique amino terminus of spastin and atlastin (10,75). Current experiments are aimed at evaluating these mechanistic possibilities.

Through various protein-protein interactions, M1 spastin has been proposed to coordinate microtubule severing with membrane remodeling during axonal branch formation (12) and pruning (7). Interestingly, this latter process reportedly involves localized inhibition of FAT (7). It may be that M1 spastin inhibits FAT by promoting localized CK2 activation and phosphorylation of motor proteins.

Collectively, our data from experiments in isolated axoplasm and cultured mammalian cells support a model where mutant M1 spastin proteins promote aberrant CK2 activation. Active CK2 would in turn phosphorylate and inhibit the major motor proteins conventional kinesin and CDyn, ultimately promoting FAT deficits that would impact the mobilization and distribution of cellular organelles at specific neuronal subdomains. Additional experiments will be needed to directly address specific motor proteins and MBO cargoes affected by mutant M1 spastins, as well as additional CK2 substrates relevant to axonal degeneration in HSP (72,76).

Most importantly, our findings may offer a novel avenue toward treatment of the disease. Relevant to this idea is the availability of cell-permeable, highly selective CK2 inhibitors

that effectively access the nervous system (77). Restoring CK2 activity to its normal levels, without compromising its basic functions, may correct FAT deficits and thereby halt axonal degeneration in *SPG4*-HSP patients.

Materials and Methods

Reagents and antibodies

Kinase and phosphatase inhibitors were from Calbiochem. Lipofectamine 2000 was from Invitrogen. Recombinant BDNF was from Alomone Labs. All other chemical reagents were from Sigma, unless stated otherwise. Antibodies were as follows:anti-spastin (clone 6c6, Santa Cruz #sc-81624), anti-acetylated tubulin (Sigma T-6793); anti-tyrosinated Tubulin (Millipore, Mab1864); anti-β tubulin (Abcam, Ab6046); anti-GM130 (Abcam ab52649), anti-GAPDH (Abcam ab8245), anti-kinesin heavy chain antibody [H2 clone) (32)], anti-kinesin light chain [63-90 clone, (78)], and anti-dynein intermediate chain [74.1 clone; from Santa Cruz #-13524; (40)]. Anti-CK2α/α' polyclonal antibody was a generous gift from Dr. D. Litchfield (University of Western Ontario, CA).

In vitro translation

Myc-tagged cDNA constructs encoding M1 and M87 isoforms of mutant human spastins were subcloned in mammalian pcDNA3.1 plasmid vector. Recombinant spastin polypeptides were produced by *in vitro* transcription/translation (Promega; TnT T7 coupled Reticulocyte Lysate system), as in our prior studies (9,36). Briefly, purified plasmids (2 μg) were transcribed in a 50μl reaction, following the manufacturer's procedures. To ensure similar levels of spastin protein perfusion, parallel reactions were performed using ^{35}S-labeled methionine (Amersham), and relative spastin levels quantified using a Typhoon phospho-imager scanner (Amersham/Molecular Dynamics). *In vitro* translated products were centrifuged to eliminate translation machinery and supernatants containing mutant spastins were perfused into isolated axoplasms at a final concentration of approximately 5–10 nM.

Vesicle motility assays in isolated squid axoplasm

Axoplasms were extruded from giant axons of the squid *Loligo pealeii*, provided at the Marine Biological Laboratory (30). *In vitro* translated spastin polypeptides were diluted into X/2 buffer (175 mM potassium aspartate, 65 mM taurine, 35 mM betaine, 25 mM glycine, 10 mM HEPES, 6.5 mM $MgCl_2$, 5 mM EGTA, 1.5 mM $CaCl_2$, 0.5 mM glucose, pH 7.2) supplemented with 5 mM ATP. After addition to perfusion chambers, axoplasms were analyzed on a Zeiss Axiomat microscope with a 100X, 1.3 n.a. objective, and DIC optics. A Hamamatsu Argus 20 and Model 2400 CCD camera was used for image processing. Membrane-bounded organelle (MBOs) velocities were measured with a Photonics Microscopy C2117 video manipulator (Hamamatsu) (30). Velocity measurements obtained 30–50 min after perfusion were analyzed by ANOVA followed by post-hoc Student-Newman-Keul's test (Supplementary Material, Table S1).

Mammalian cell cultures

RFL-6 rat fibroblasts were cultured as previously described (63). For primary cultures of rat cortical neurons (49), rat cortices were dissected from embryonic (E18) rat cortex and dissociated using trypsin. Cells were plated at a density of 25–35,000 per dish onto 35 mm petri dishes where a 14 mm diameter hole had been drilled and a poly-L-lysine (P2636, Sigma)-coated glass coverslip (In Vitro Scientific) was adhered. Neurons were maintained in DMEM/astroglia-conditioned media and transfected at 2 DIV, as before (79). Morphological analysis of cells was performed 24-h post-transfection.

Generation of M1-STOP and M87-STOP cell lines

SH-SY5Y neuroblastoma cell monoclones stably expressing mutant M87-STOP (D5 clone) or M1-STOP spastin (D2 clone) were established using lentivirus-mediated infection and clonal selection methods. A description of these procedures and a characterization of these cells are provided in Supplementary Material, (Figs S1-3). Due to higher stability of mutant M1 proteins relative to M87 proteins, transgenic mutant spastin protein levels are higher for M1-STOP cells than for M87-STOP cells (see Supplementary Material, Fig. S2B).

Metabolic labeling experiments

M1-STOP and M87-STOP cells were plated in 10cm diameter plastic dishes coated with poly-L-lysine and maintained in DMEM plus 10% fetal bovine serum. Cells were differentiated by adding 10 μM retinoic acid for 5–6 days, then switched to serum-free DMEM supplemented with 25ng/ml BDNF for 5 days (80). At day 5, ¾ of media were replaced with phosphate-free DMEM plus BDNF. For metabolic labeling, 1mCi ^{32}P phosphate (ICN) was added per dish. After 4-h incubation, media were discarded and cells lysed in 1ml of ROLB buffer [10mM Hepes, pH 7.4, 0.5% Triton X-100, 80mM beta-glycerophosphate, 50mM sodium fluoride, 2mM sodium orthovanadate, 100nM staurosporine, 100nM K252a, 50nM okadaic acid, 50nM microcystin, 100mM potassium phosphate, mammalian protease inhibitor cocktail (1/100 dilution; Sigma) and of phosphatase inhibitor cocktail (1/100 dilution; Calbiochem), pH 7.4]. Aliquots (10 μl) of each cell lysate were precipitated using 15% TCA and ^{32}P incorporation into proteins determined by scintillation counting. Equal amounts of TCA-precipitated ^{32}P counts were used to sequentially immunoprecipitate conventional kinesin and cytoplasmic dynein (CDyn) using 4μg of H2 and 74.1 antibodies, respectively (81). Immunoprecipitates were separated by SDS-PAGE, gels dried and ^{32}P incorporation in specific protein bands quantified using phospho-imager scanning, as before (82).

Immunoblotting

Cell lysates were run on 4–12% Bis/Tris gels (Invitrogen) and proteins transferred to Immobilon-P membranes (Millipore). Membranes were blocked at RT for 60 min with 5% milk in TBS. Primary antibodies were diluted in TBS containing 1% BSA and incubated with primary antibodies overnight at 4C. After washing, membranes were incubated with HRP-conjugated secondary antibodies from (Jackson Immunoresearch) and proteins visualized using chemiluminescence, as before (39).

CK2 activity assays

CK2 kinase activity assays were done as previously described, with minor modifications (83,84). Briefly, M1-STOP and M87-STOP cells were collected in ROLB buffer. Lysates were clarified through centrifugation and normalized to 1μg protein/μl.

Aliquots of each lysate (3 μg) were incubated with a highly specific CK2 peptide substrate (CK2pept: RRREEETEEE; from Sigma Genosys) in 30μl of kinase buffer [KB: 25mM HEPES, 12mM MgCl, 100mM NaCl, 50nM okadaic acid, 200nM mycrocystin, and mammalian protease inhibitor cocktail (1/100 dilution), pH 7.4]. Kinase reactions were started by addition of ^{32}P-radiolabelled ATP (100 μM), and aliquots spotted on P81 phosphocellulose paper in triplicates at various time points. After extensive washing in 100 mM phosphoric acid, ^{32}P incorporation into CK2pept was determined using a scintillation counter. Cell lysates incubated in the absence of CK2pept were used for both background controls and normalization.

Transfection procedures

Adherent RFL-6 cells were plated at a density of 10,000 cells per 1.53 cm^2 dish. After 48 h, cells were transfected using 1 μg of plasmid cDNA and 2.5 μl of Lipofectamine 2000 per dish, resulting in 10–15% transfection efficiency (85). Primary cortical neurons were transfected using a Cellaxess CX1 device (Cellectricon), following a slightly modified version of our procedures (86). This device transfects by electroporating small groups or 'patches' of cells adhered to a substratum. Specifically, 18μg of cDNA plasmids encoding M1-C448Yand RFP (with IRES), M87-C448Yand RFP (with IRES), or RFP alone were used per electroporation, with three separate patches of cells transfected per dish, thus allowing a transfection average of 5–10 neurons per dish. Under these experimental settings, 30 cells per condition per experiment were used for analysis. Only transfected neurons on the periphery of each patch were analyzed, because neurons in the center of patch often died as a result of the electroporation, which is stronger in the center of the patch. For analysis of mitochondrial distribution in Figure 7, an average of 100 cells per condition per experiment were analyzed. For vesicle trafficking experiments in Figures 3A and B and 6B and C, SH-SY5Y cells were transfected using a Nucleofector device, as before (49).

Analysis of RFP-tagged synaptophysin motility

Following Nucleofector-based transfection of RFP-tagged synaptophysin, SH-SY5Y cells were plated at a density of 15,000 cells per 1.53cm^2 dish. Two days after transfection, movies of RFP-synaptophysin-containing vesicles were generated by capturing 5 frames per second for a total length of 20 seconds (87). The initial 5 μm of neurites proximal to the cell body were excluded from this analysis. Vesicles moving $>$30 μm during the overall length of a movie were considered mobile, while those moving $<$30 μm were considered stationary. An average of 30 cells per experimental group were analyzed.

Analysis of Golgi and mitochondrial distribution

Golgi dispersion was evaluated by immunofluorescence using anti-GM130 antibody, a cis-Golgi marker (88). Images were taken with an Axiovert 200 inverted microscope (Zeiss) using a 63X objective. Pictures selected for quantitation did not contain saturated or underexposed pixels in the region of interest. Together with Axiovision 4.6 software, anti-GM130-derived immunofluorescence and GFP were used to measure the Golgi apparatus and total cell surface areas, respectively. Mitochondria were visualized by incubating living cells with Green Mitotracker® (20 nM) for 20 min at 37°C, as described before (89). The mitochondrial array of a cell was classified as 'clustered' when more than half of the total Mitotracker-positive structures localized asymmetrically on one side of the nucleus. The mitochondrial array of a cell not fitting this description was classified as 'dispersed.' Quantitative values in Figures 3D, 6E, 7E and L involved a minimum of 30 independent measurements per experimental condition.

Immunocytochemistry-based analysis of microtubules

SH-SY5Y cells were simultaneously fixed and permeabilized using microtubule-stabilizing buffer (PHEM: 60 mM Pipes, 25 mM Hepes, 10 mM EGTA 2 mM MgCl2 2mM, Paraformaldehyde 4%, 0.125% glutaraldehyde, 0.1% Triton. pH 6.9). Quantitative immunofluorescence-based analysis of acetylated and tyrosinated microtubules was done as described in our prior work (49).

Pharmacological CK2 inhibition in cultured mammalian cells

One hour after transfection, RFL-6 fibroblasts, SH-SY5Y cells, and primary cortical neurons were treated with vehicle control (DMSO) or with the highly specific CK2 inhibitor TBCA [Calbiochem# 218710, 20 μM (90)]. After 24 h, cells were fixed and processed for image analysis.

Statistical analyses

Statistical comparisons were obtained by using SPSS 20 (IBM) and Excel (Microsoft). Data represent mean ± SD. Mean differences were considered significant at $P \leq 0.05$ level. Multiple group comparisons were performed by one-way ANOVA followed by Bonferroni post hoc. For pair comparisons, Student's *t*-tests were used.

Supplementary Material

Supplementary Material is available at *HMG* online.

Acknowledgements

The authors would like to thank Joanna Solowska (Drexel University) and Erin Dongyang (UIC) for preparation of spastin cDNA constructs, and personnel at the Marine Resources Center of MBL for assistance with squid. GM, STB, and PWB were supported by grants from the National Institutes of Health. PWB and LQ were supported by two Pennsylvania Department of Health CURE grants issued through Drexel University College of Medicine. LL was supported by a Dean's Fellowship for Excellence in Collaborative Research Training from Drexel University's Graduate School. PWB is the 2017 recipient of the Advanced Scholarship for Research into Hereditary Spastic Paraplegia and Related Diseases from the Tom Wahlig Foundation.

Conflict of Interest statement. None declared.

Funding

National Institutes of Health NS066942A, NS096642, NS023868, NS041170, NS28785, Pennsylvania Department of Health CURE grants issued through Drexel University College of Medicine,

Dean's Fellowship for Excellence in Collaborative Research Training from Drexel University's Graduate School, Tom Wahlig Foundation.

References

1. Deluca, G.C., Ebers, G.C. and Esiri, M.M. (2004) The extent of axonal loss in the long tracts in hereditary spastic paraplegia. *Neuropathol. Appl. Neurobiol.*, **30**, 576–584.
2. Blackstone, C., O'Kane, C.J. and Reid, E. (2011) Hereditary spastic paraplegias: membrane traffic and the motor pathway. *Nat. Rev. Neurosci.*, **12**, 31–42.
3. Solowska, J.M. and Baas, P.W. (2015) Hereditary spastic paraplegia SPG4: what is known and not known about the disease. *Brain*, **138**, 2471–2484.
4. Fink, J.K. (2013) Hereditary spastic paraplegia: clinico-pathologic features and emerging molecular mechanisms. *Acta Neuropathol.*, **126**, 307–328.
5. Errico, A., Ballabio, A. and Rugarli, E.I. (2002) Spastin, the protein mutated in autosomal dominant hereditary spastic paraplegia, is involved in microtubule dynamics. *Hum. Mol. Genet.*, **11**, 153–163.
6. Baas, P.W., Karabay, A. and Qiang, L. (2005) Microtubules cut and run. *Trends Cell Biol.*, **15**, 518–524.
7. Brill, M.S., Kleele, T., Ruschkies, L., Wang, M., Marahori, N.A., Reuter, M.S., Hausrat, T.J., Weigand, E., Fisher, M., Ahles, A. *et al.* (2016) Branch-Specific Microtubule Destabilization Mediates Axon Branch Loss during Neuromuscular Synapse Elimination. *Neuron*, **92**, 845–856.
8. Claudiani, P., Riano, E., Errico, A., Andolfi, G. and Rugarli, E.I (2005) Spastin subcellular localization is regulated through usage of different translation start sites and active export from the nucleus. *Exp. Cell Res.*, **309**, 358–369.
9. Solowska, J.M., Morfini, G., Falnikar, A., Himes, B.T., Brady, S.T., Huang, D. and Baas, P.W. (2008) Quantitative and functional analyses of spastin in the nervous system: implications for hereditary spastic paraplegia. *J. Neurosci.*, **28**, 2147–2157.
10. Sanderson, C.M., Connell, J.W., Edwards, T.L., Bright, N.A., Duley, S., Thompson, A., Luzio, J.P. and Reid, E. (2006) Spastin and atlastin, two proteins mutated in autosomal-dominant hereditary spastic paraplegia, are binding partners. *Hum. Mol. Genet.*, **15**, 307–318.
11. Park, S.H., Zhu, P.P., Parker, R.L. and Blackstone, C. (2010) Hereditary spastic paraplegia proteins REEP1, spastin, and atlastin-1 coordinate microtubule interactions with the tubular ER network. *J. Clin. Invest.*, **120**, 1097–1110.
12. Connell, J.W., Lindon, C., Luzio, J.P. and Reid, E. (2009) Spastin couples microtubule severing to membrane traffic in completion of cytokinesis and secretion. *Traffic*, **10**, 42–56.
13. Wharton, S.B., McDermott, C.J., Grierson, A.J., Wood, J.D., Gelsthorpe, C., Ince, P.G. and Shaw, P.J. (2003) The cellular and molecular pathology of the motor system in hereditary spastic paraparesis due to mutation of the spastin gene. *J. Neuropathol. Exp. Neurol.*, **62**, 1166–1177.
14. Soderblom, C. and Blackstone, C. (2006) Traffic accidents: molecular genetic insights into the pathogenesis of the hereditary spastic paraplegias. *Pharmacol. Ther.*, **109**, 42–56.
15. Reid, E., Kloos, M., Ashley-Koch, A., Hughes, L., Bevan, S., Svenson, I.K., Graham, F.L., Gaskell, P.C., Dearlove, A., Pericak-Vance, M.A. *et al.* (2002) A Kinesin Heavy Chain (KIF5A) Mutation in Hereditary Spastic Paraplegia (SPG10). *Am. J. Hum. Genet.*, **71**, 1189–1194.
16. Wali, G., Sutharsan, R., Fan, Y., Stewart, R., Tello Velasquez, J., Sue, C.M., Crane, D.I. and Mackay-Sim, A. (2016) Mechanism of impaired microtubule-dependent peroxisome trafficking and oxidative stress in SPAST-mutated cells from patients with Hereditary Spastic Paraplegia. *Sci. Rep.*, **6**, 27004.
17. Denton, K.R., Lei, L., Grenier, J., Rodionov, V., Blackstone, C. and Li, X.J. (2014) Loss of spastin function results in disease-specific axonal defects in human pluripotent stem cell-based models of hereditary spastic paraplegia. *Stem Cells*, **32**, 414–423.
18. Fuerst, J.C., Henkel, A.W., Stroebel, A., Welzel, O., Groemer, T.W., Kornhuber, J. and Bonsch, D. (2011) Distinct intracellular vesicle transport mechanisms are selectively modified by spastin and spastin mutations. *J. Cell Physiol.*, **226**, 362–368.
19. Kasher, P.R., De Vos, K.J., Wharton, S.B., Manser, C., Bennett, E.J., Bingley, M., Wood, J.D., Milner, R., McDermott, C.J., Miller, C.C. *et al.* (2009) Direct evidence for axonal transport defects in a novel mouse model of mutant spastin-induced hereditary spastic paraplegia (HSP) and human HSP patients. *J. Neurochem.*, **110**, 34–44.
20. Stone, M.C., Rao, K., Gheres, K.W., Kim, S., Tao, J., La Rochelle, C., Folker, C.T., Sherwood, N.T. and Rolls, M.M. (2012) Normal spastin gene dosage is specifically required for axon regeneration. *Cell Rep.*, **2**, 1340–1350.
21. Havlicek, S., Kohl, Z., Mishra, H.K., Prots, I., Eberhardt, E., Denguir, N., Wend, H., Plotz, S., Boyer, L., Marchetto, M.C. *et al.* (2014) Gene dosage-dependent rescue of HSP neurite defects in SPG4 patients' neurons. *Hum. Mol. Genet.*, **23**, 2527–2541.
22. Charvin, D., Cifuentes-Diaz, C., Fonknechten, N., Joshi, V., Hazan, J., Melki, J. and Betuing, S. (2003) Mutations of SPG4 are responsible for a loss of function of spastin, an abundant neuronal protein localized in the nucleus. *Hum. Mol. Genet.*, **12**, 71–78.
23. Salinas, S., Carazo-Salas, R.E., Proukakis, C., Schiavo, G. and Warner, T.T. (2007) Spastin and microtubules: Functions in health and disease. *J. Neurosci. Res.*, **85**, 2778–2782.
24. Shoukier, M., Neesen, J., Sauter, S.M., Argyriou, L., Doerwald, N., Pantakani, D.V. and Mannan, A.U. (2009) Expansion of mutation spectrum, determination of mutation cluster regions and predictive structural classification of SPAST mutations in hereditary spastic paraplegia. *Eur. J. Hum. Genet.*, **17**, 187–194.
25. Gibbs, K.L., Greensmith, L. and Schiavo, G. (2015) Regulation of Axonal Transport by Protein Kinases. *Trends Biochem. Sci.*, **40**, 597–610.
26. Morfini, G.A., Burns, M., Binder, L.I., Kanaan, N.M., LaPointe, N., Bosco, D.A., Brown, R.H., Jr., Brown, H., Tiwari, A., Hayward, L. *et al.* (2009) Axonal transport defects in neurodegenerative diseases. *J. Neurosci.*, **29**, 12776–12786.
27. Svenson, I.K., Ashley-Koch, A.E., Gaskell, P.C., Riney, T.J., Cumming, W.J., Kingston, H.M., Hogan, E.L., Boustany, R.M., Vance, J.M., Nance, M.A. *et al.* (2001) Identification and expression analysis of spastin gene mutations in hereditary spastic paraplegia. *Am. J. Hum. Genet.*, **68**, 1077–1085.
28. Abrahamsen, G., Fan, Y., Matigian, N., Wali, G., Bellette, B., Sutharsan, R., Raju, J., Wood, S.A., Veivers, D., Sue, C.M. *et al.* (2013) A patient-derived stem cell model of hereditary spastic paraplegia with SPAST mutations. *Dis. Model Mech.*, **6**, 489–502.
29. Molon, A., Di Giovanni, S., Chen, Y.W., Clarkson, P.M., Angelini, C., Pegoraro, E. and Hoffman, E.P. (2004) Large-scale disruption of microtubule pathways in morphologically normal human spastin muscle. *Neurology*, **62**, 1097–1104.

30. Song, Y., Kang, M., Morfini, G. and Brady, S.T. (2016) Fast axonal transport in isolated axoplasm from the squid giant axon. *Methods Cell Biol.*, **131**, 331–348.
31. Morfini, G., Pigino, G., Mizuno, N., Kikkawa, M. and Brady, S.T. (2007) Tau binding to microtubules does not directly affect microtubule-based vesicle motility. *J. Neurosci. Res.*, **85**, 2620–2630.
32. Brady, S.T., Pfister, K.K. and Bloom, G.S. (1990) A monoclonal antibody against kinesin inhibits both anterograde and retrograde fast axonal transport in squid axoplasm. *Proc. Nat. Acad. Sci. USA*, **87**, 1061–1065.
33. Gilbert, S.P. and Sloboda, R.D. (1989) A squid dynein isoform promotes axoplasmic vesicle translocation. *J. Cell Biol.*, **109**, 2379–2394.
34. Fonknechten, N., Mavel, D., Byrne, P., Davoine, C.S., Cruaud, C., Bonsch, D., Samson, D., Coutinho, P., Hutchinson, M., McMonagle, P. *et al.* (2000) Spectrum of SPG4 mutations in autosomal dominant spastic paraplegia. *Hum. Mol. Genet.*, **9**, 637–644.
35. White, S.R., Evans, K.J., Lary, J., Cole, J.L. and Lauring, B. (2007) Recognition of C-terminal amino acids in tubulin by pore loops in Spastin is important for microtubule severing. *J. Cell Biol.*, **176**, 995–1005.
36. Szebenyi, G., Morfini, G., Babcock, A., Gould, M., Selkoe, K., Stenoien, D., Young, M., Faber, P., MacDonald, M., McPhaul, M. *et al.* (2003) Neuropathogenic forms of huntingtin and androgen receptor inhibit fast axonal transport. *Neuron*, **40**, 41–52.
37. Feiguin, F., Ferreira, A., Kosik, K.S. and Caceres, A. (1994) Kinesin-mediated organelle translocation revealed by specific cellular manipulations. *J. Cell Biol.*, **127**, 1021–1039.
38. Jaarsma, D. and Hoogenraad, C.C. (2015) Cytoplasmic dynein and its regulatory proteins in Golgi pathology in nervous system disorders. *Front. Neurosci.*, **9**, 397.
39. DeBoer, S.R., You, Y., Szodorai, A., Kaminska, A., Pigino, G., Nwabuisi, E., Wang, B., Estrada-Hernandez, T., Kins, S., Brady, S.T. *et al.* (2008) Conventional kinesin holoenzymes are composed of heavy and light chain homodimers. *Biochemistry*, **47**, 4535–4543.
40. Brill, L.B. 2nd and Pfister, K.K. (2000) Biochemical and molecular analysis of the mammalian cytoplasmic dynein intermediate chain. *Methods*, **22**, 307–316.
41. Pigino, G., Morfini, G., Atagi, Y., Deshpande, A., Yu, C., Jungbauer, L., LaDu, M., Busciglio, J. and Brady, S. (2009) Disruption of fast axonal transport is a pathogenic mechanism for intraneuronal amyloid beta. *Proc. Natl Acad. Sci. U S A*, **106**, 5907–5912.
42. Morfini, G., Szebenyi, G., Richards, B. and Brady, S.T. (2001) Regulation of kinesin: implications for neuronal development. *Dev. Neurosci.*, **23**, 364–376.
43. Donelan, M.J., Morfini, G., Julyan, R., Sommers, S., Hays, L., Kajio, H., Briaud, I., Easom, R.A., Molkentin, J.D., Brady, S.T. *et al.* (2002) Ca2+-dependent dephosphorylation of kinesin heavy chain on beta-granules in pancreatic beta-cells. Implications for regulated beta-granule transport and insulin exocytosis. *J. Biol. Chem.*, **277**, 24232–24242.
44. Karki, S., Tokito, M.K. and Holzbaur, E.L. (1997) Casein kinase II binds to and phosphorylates cytoplasmic dynein. *J. Biol. Chem.*, **272**, 5887–5891.
45. Schafer, B., Gotz, C. and Montenarh, M. (2008) The kinesin I family member KIF5C is a novel substrate for protein kinase CK2. *Biochem. Biophys. Res. Commun.*, **375**, 179–183.
46. Pagano, M.A., Poletto, G., Di Maira, G., Cozza, G., Ruzzene, M., Sarno, S., Bain, J., Elliott, M., Moro, S., Zagotto, G. *et al.* (2007) Tetrabromocinnamic acid (TBCA) and related compounds represent a new class of specific protein kinase CK2 inhibitors. *Chembiochem.*, **8**, 129–139.
47. Pagano, M.A., Meggio, F., Ruzzene, M., Andrzejewska, M., Kazimierczuk, Z. and Pinna, L.A. (2004) 2-Dimethylamino-4,5,6,7-tetrabromo-1H-benzimidazole: a novel powerful and selective inhibitor of protein kinase CK2. *Biochem. Biophys. Res. Commun.*, **321**, 1040–1044.
48. Litchfield, D.W. (2003) Protein kinase CK2: structure, regulation and role in cellular decisions of life and death. *Biochem. J.*, **369**, 1–15.
49. Leo, L., Yu, W., D'Rozario, M., Waddell, E.A., Marenda, D.R., Baird, M.A., Davidson, M.W., Zhou, B., Wu, B., Baker, L. *et al.* (2015) Vertebrate Fidgetin Restrains Axonal Growth by Severing Labile Domains of Microtubules. *Cell Rep.*, **12**, 1723–1730.
50. Schickel, J., Beetz, C., Frommel, C., Heide, G., Sasse, A., Hemmerich, P. and Deufel, T. (2006) Unexpected pathogenic mechanism of a novel mutation in the coding sequence of SPG4 (spastin). *Neurology*, **66**, 421–423.
51. Depienne, C., Fedirko, E., Forlani, S., Cazeneuve, C., Ribai, P., Feki, I., Tallaksen, C., Nguyen, K., Stankoff, B., Ruberg, M. *et al.* (2007) Exon deletions of SPG4 are a frequent cause of hereditary spastic paraplegia. *J. Med. Genet.*, **44**, 281–284.
52. Fink, J.K. and Rainier, S. (2004) Hereditary spastic paraplegia: spastin phenotype and function. *Arch. Neurol.*, **61**, 830–833.
53. Riano, E., Martignoni, M., Mancuso, G., Cartelli, D., Crippa, F., Toldo, I., Siciliano, G., Di Bella, D., Taroni, F., Bassi, M.T. *et al.* (2009) Pleiotropic effects of spastin on neurite growth depending on expression levels. *J. Neurochem.*, **108**, 1277–1288.
54. Solowska, J.M., Garbern, J.Y. and Baas, P.W. (2010) Evaluation of loss of function as an explanation for SPG4-based hereditary spastic paraplegia. *Hum. Mol. Genet.*, **19**, 2767–2779.
55. Jonsson, P.A., Ernhill, K., Andersen, P.M., Bergemalm, D., Brannstrom, T., Gredal, O., Nilsson, P. and Marklund, S.L. (2004) Minute quantities of misfolded mutant superoxide dismutase-1 cause amyotrophic lateral sclerosis. *Brain*, **127**, 73–88.
56. Benn, C.L., Landles, C., Li, H., Strand, A.D., Woodman, B., Sathasivam, K., Li, S.H., Ghazi-Noori, S., Hockly, E., Faruque, S.M. *et al.* (2005) Contribution of nuclear and extranuclear polyQ to neurological phenotypes in mouse models of Huntington's disease. *Hum. Mol. Genet.*, **14**, 3065–3078.
57. Boone, P.M., Yuan, B., Campbell, I.M., Scull, J.C., Withers, M.A., Baggett, B.C., Beck, C.R., Shaw, C.J., Stankiewicz, P., Moretti, P. *et al.* (2014) The Alu-rich genomic architecture of SPAST predisposes to diverse and functionally distinct disease-associated CNV alleles. *Am. J. Hum. Genet.*, **95**, 143–161.
58. Julien, C., Lissouba, A., Madabattula, S., Fardghassemi, Y., Rosenfelt, C., Androschuk, A., Strautman, J., Wong, C., Bysice, A., O'Sullivan, J. *et al.* (2016) Conserved pharmacological rescue of hereditary spastic paraplegia-related phenotypes across model organisms. *Hum. Mol. Genet.*, **25**, 1088–1099.
59. Tarrade, A., Fassier, C., Courageot, S., Charvin, D., Vitte, J., Peris, L., Thorel, A., Mouisel, E., Fonknechten, N., Roblot, N. *et al.* (2006) A mutation of spastin is responsible for swellings and impairment of transport in a region of axon characterized by changes in microtubule composition. *Hum. Mol. Genet.*, **15**, 3544–3558.
60. Trotta, N., Orso, G., Rossetto, M.G., Daga, A. and Broadie, K. (2004) The hereditary spastic paraplegia gene, spastin,

regulates microtubule stability to modulate synaptic structure and function. *Curr. Biol.*, **14**, 1135–1147.
61. Sherwood, N.T., Sun, Q., Xue, M., Zhang, B. and Zinn, K. (2004) Drosophila spastin regulates synaptic microtubule networks and is required for normal motor function. *PLoS Biol.*, **2**, e429.
62. Orso, G., Martinuzzi, A., Rossetto, M.G., Sartori, E., Feany, M. and Daga, A. (2005) Disease-related phenotypes in a Drosophila model of hereditary spastic paraplegia are ameliorated by treatment with vinblastine. *J. Clin. Invest.*, **115**, 3026–3034.
63. Solowska, J.M., D'Rozario, M., Jean, D.C., Davidson, M.W., Marenda, D.R. and Baas, P.W. (2014) Pathogenic mutation of spastin has gain-of-function effects on microtubule dynamics. *J. Neurosci.*, **34**, 1856–1867.
64. Draberova, E., Vinopal, S., Morfini, G., Liu, P.S., Sladkova, V., Sulimenko, T., Burns, M.R., Solowska, J., Kulandaivel, K., de Chadarevian, J.P. *et al.* (2011) Microtubule-severing ATPase spastin in glioblastoma: increased expression in human glioblastoma cell lines and inverse roles in cell motility and proliferation. *J. Neuropathol. Exp. Neurol.*, **70**, 811–826.
65. Qiang, L., Yu, W., Liu, M., Solowska, J.M. and Baas, P.W. (2010) Basic fibroblast growth factor elicits formation of interstitial axonal branches via enhanced severing of microtubules. *Mol. Biol. Cell*, **21**, 334–344.
66. Connell, J.W., Allison, R. and Reid, E. (2016) Quantitative Gait Analysis Using a Motorized Treadmill System Sensitively Detects Motor Abnormalities in Mice Expressing ATPase Defective Spastin. *PLoS One.*, **11**, e0152413. doi: 10.1371/journal.pone.0152413.
67. McDermott, C.J., Grierson, A.J., Wood, J.D., Bingley, M., Wharton, S.B., Bushby, K.M. and Shaw, P.J. (2003) Hereditary spastic paraparesis: disrupted intracellular transport associated with spastin mutation. *Ann. Neurol.*, **54**, 748–759.
68. Kanaan, N.M., Morfini, G.A., LaPointe, N.E., Pigino, G.F., Patterson, K.R., Song, Y., Andreadis, A., Fu, Y., Brady, S.T. and Binder, L.I. (2011) Pathogenic forms of tau inhibit kinesin-dependent axonal transport through a mechanism involving activation of axonal phosphotransferases. *J. Neurosci.*, **31**, 9858–9868.
69. Morfini, G.A., Bosco, D.A., Brown, H., Gatto, R., Kaminska, A., Song, Y., Molla, L., Baker, L., Marangoni, M.N., Berth, S. *et al.* (2013) Inhibition of fast axonal transport by pathogenic SOD1 involves activation of p38 MAP kinase. *PLoS One*, **8**, e65235.
70. Gyenis, L. and Litchfield, D.W. (2008) The emerging CK2 interactome: insights into the regulation and functions of CK2. *Mol. Cell Biochem.*, **316**, 5–14.
71. Olsten, M.E., Weber, J.E. and Litchfield, D.W. (2005) CK2 interacting proteins: emerging paradigms for CK2 regulation?. *Mol. Cell Biochem.*, **274**, 115–124.
72. Olsten, M.E. and Litchfield, D.W. (2004) Order or chaos? An evaluation of the regulation of protein kinase CK2. *Biochem. Cell Biol.*, **82**, 681–693.
73. Pinna, L.A. (2003) The raison d'etre of constitutively active protein kinases: the lesson of CK2. *Acc. Chem. Res.*, **36**, 378–384.
74. Gotz, C., Kartarius, S., Scholtes, P. and Montenarh, M. (2000) Binding domain for p21(WAF1) on the polypeptide chain of the protein kinase CK2 beta-subunit. *Biochem. Biophys. Res. Commun.*, **268**, 882–885.
75. Evans, K., Keller, C., Pavur, K., Glasgow, K., Conn, B. and Lauring, B. (2006) Interaction of two hereditary spastic paraplegia gene products, spastin and atlastin, suggests a common pathway for axonal maintenance. *Proc. Natl Acad. Sci. U S A*, **103**, 10666–10671.
76. Rasband, M.N. (2008) Na+ channels get anchored. . .with a little help. *J. Cell Biol.*, **183**, 975–977.
77. Pagano, M.A., Cesaro, L., Meggio, F. and Pinna, L.A. (2006) Protein kinase CK2: a newcomer in the 'druggable kinome'. *Biochem. Soc. Trans.*, **34**, 1303–1306.
78. Stenoien, D.S. and Brady, S.T. (1997) Immunochemical analysis of kinesin light chain function. *Molec. Biol. Cell*, **8**, 675–689.
79. Sudo, H. and Baas, P.W. (2010) Acetylation of microtubules influences their sensitivity to severing by katanin in neurons and fibroblasts. *J. Neurosci.*, **30**, 7215–7226.
80. Encinas, M., Iglesias, M., Liu, Y., Wang, H., Muhaisen, A., Cena, V., Gallego, C. and Comella, J.X. (2000) Sequential treatment of SH-SY5Y cells with retinoic acid and brain-derived neurotrophic factor gives rise to fully differentiated, neurotrophic factor-dependent, human neuron-like cells. *J. Neurochem.*, **75**, 991–1003.
81. Kang, M., Baker, L., Song, Y., Brady, S.T. and Morfini, G. (2016) Biochemical analysis of axon-specific phosphorylation events using isolated squid axoplasms. *Methods Cell Biol.*, **131**, 199–216.
82. Morfini, G., Pigino, G. and Brady, S.T. (2007) Approaches to kinesin-1 phosphorylation. *Methods Mol. Biol.*, **392**, 51–69.
83. Ruzzene, M., Penzo, D. and Pinna, L.A. (2002) Protein kinase CK2 inhibitor 4,5,6,7-tetrabromobenzotriazole (TBB) induces apoptosis and caspase-dependent degradation of haematopoietic lineage cell-specific protein 1 (HS1) in Jurkat cells. *Biochem. J.*, **364**, 41–47.
84. Arevalo, M.A. and Rodriguez-Tebar, A. (2006) Activation of casein kinase II and inhibition of phosphatase and tensin homologue deleted on chromosome 10 phosphatase by nerve growth factor/p75NTR inhibit glycogen synthase kinase-3beta and stimulate axonal growth. *Mol. Biol. Cell*, **17**, 3369–3377.
85. Yu, W., Solowska, J.M., Qiang, L., Karabay, A., Baird, D. and Baas, P.W. (2005) Regulation of microtubule severing by katanin subunits during neuronal development. *J. Neurosci.*, **25**, 5573–5583.
86. Lin, S., Liu, M., Mozgova, O.I., Yu, W. and Baas, P.W. (2012) Mitotic motors coregulate microtubule patterns in axons and dendrites. *J. Neurosci.*, **32**, 14033–14049.
87. Tang, Y., Scott, D.A., Das, U., Edland, S.D., Radomski, K., Koo, E.H. and Roy, S. (2012) Early and selective impairments in axonal transport kinetics of synaptic cargoes induced by soluble amyloid beta-protein oligomers. *Traffic*, **13**, 681–693.
88. Nakamura, N., Rabouille, C., Watson, R., Nilsson, T., Hui, N., Slusarewicz, P., Kreis, T.E. and Warren, G. (1995) Characterization of a cis-Golgi matrix protein, GM130. *J. Cell Biol.*, **131**, 1715–1726.
89. Samudio, I., Konopleva, M., Hail, N., Jr., Shi, Y.X., McQueen, T., Hsu, T., Evans, R., Honda, T., Gribble, G.W., Sporn, M. *et al.* (2005) 2-Cyano-3,12-dioxooleana-1,9-dien-28-imidazolide (CDDO-Im) directly targets mitochondrial glutathione to induce apoptosis in pancreatic cancer. *J. Biol. Chem.*, **280**, 36273–36282.
90. Kang, K.R. and Chung, S.I. (2003) Protein kinase CK2 phosphorylates and interacts with deoxyhypusine synthase in HeLa cells. *Exp. Mol. Med.*, **35**, 556–564.